

MHD induced alpha particle loss in TFTR

S.J. Zweben, D.S. Darrow, E.D. Fredrickson,
G. Taylor, S. von Goeler, R.B. White
Princeton Plasma Physics Laboratory, Princeton University,
Princeton, New Jersey,
United States of America

Abstract. Increases in alpha particle loss due to MHD activity in TFTR were observed for both coherent modes and transient reconnection events using an array of scintillator detectors near the wall. The magnitude of the coherent MHD induced alpha loss was normally comparable to the MHD quiescent first orbit or TF ripple loss, but the magnitude of the alpha loss during reconnection events was up to 1000 times higher than this for a short time. Modelling suggests that the coherent MHD loss mechanism will be less significant for future reactor scale DT tokamaks due to the smaller ratio of the alpha gyroradius to the minor radius.

1. Introduction

The effect of low frequency MHD activity on the confinement of 3.5 MeV alpha particles is one of the most basic issues in tokamak physics, since it involves the dynamics of single particle orbits in the presence of simple toroidal symmetry breaking perturbations. This is also a topic of interest for the development of future DT reactors, since any significant loss of alpha particle confinement could lead to a loss of alpha heating power or to an unplanned alpha particle heat load on the first wall.

This article describes measurements of MHD induced alpha particle loss made during the TFTR DT run using the lost alpha scintillator diagnostic. These observations include all the major types of plasma driven low frequency MHD activity normally observed in tokamaks, such as coherent low- n ‘tearing’ modes, sawteeth and disruptions. Since this MHD activity in TFTR is similar between DD and DT discharges [1], many of the observations are qualitatively similar to those previously reported for DD fusion products in TFTR [2]. This article does not treat the effects of alpha particle driven MHD modes such as the toroidal Alfvén eigenmode, which were observed only during a narrow range of DT operation [3]. Therefore the phenomena examined in this article are ‘single particle’ MHD–alpha interactions, and not the ‘collective’ interactions associated with a large population of alpha particles.

There are many prior experiments which relate to this subject, since fast ions have been used to heat tokamak plasmas for many years. In general, it has been found that fast ion confinement is not seriously degraded by MHD activity except during strong collective fast ion driven modes such as beam

driven fishbones or TAEs [4–6]. Such measurements were typically made by observing a reduction in the fusion product burnup or a decrease in neutron emission, whereas the present experiment describes direct observations of the alpha particle loss to the wall.

The theory of MHD–alpha interactions has been fairly well developed in the past few years, motivated in part by the DT experiments on TFTR and JET, and by the ITER project. Two basic physical interactions have been considered:

- (a) The effect of coherent low frequency helical magnetic perturbations on fast ion orbits [7–11],
- (b) The effect of sudden magnetic reconnection events on the particle transport [12–14].

These theories take into account the finite ion gyroradius and orbit size, and in some cases also the transit resonances between the ions and the MHD mode.

This article is organized as follows: Section 2 contains experimental details, including a brief review of prior experimental results, Section 3 describes the TFTR DT experimental results for alpha particle loss due to both coherent MHD and reconnection events, Section 4 describes the theoretical modelling of these results and Section 5 discusses the interpretation of these results and their implications for future tokamak experiments.

2. Experimental details and previous results

This section describes the diagnostic set-up and reviews the previous experimental results on the interactions between MHD modes and fast ions in tokamaks. All the alpha particle data in the present

article come from the TFTR lost alpha scintillator diagnostic. Since the general design and operation of this diagnostic have been described previously [15–17], only the details especially relevant to the present experiment are discussed here.

2.1. Experimental details

There were four different alpha scintillator detectors arrayed poloidally along the bottom half (ion ∇B drift direction) of the TFTR vessel at one toroidal location. All of these had a similar design, with a $0.1\text{ cm} \times 0.2\text{ cm}$ pinhole aperture in front of a $0.1\text{ cm} \times 0.7\text{ cm}$ slit which dispersed alphas according to their pitch angle and energy, and allowed them to strike a scintillator plate located inside a light-tight box. Three of these four detectors were at poloidal angles of 90° , 60° and 45° below the outer midplane with their apertures fixed in position $\approx 1\text{ cm}$ radially behind the geometrical shadow of the outer poloidal ring limiters. The fourth detector was 20° below the outer midplane, but radially movable across the outer limiter shadow [17].

These detectors responded to any large gyroradius ions which reached the scintillator plate; so in DD experiments the signal contained both 3 MeV protons and 1 MeV tritons. For the present experiments the response was almost entirely due to DT alpha particles, since there was no other comparable source of fast ions (e.g. no source of ICRF induced tail ions).

The total light emission from each scintillator was measured by photomultiplier tubes and recorded using both a slow and a fast bank of digitizers. The slow bank digitized at up to 20 kHz, while the fast bank digitized at up to 500 kHz, with analogue bandwidths of ≈ 20 and ≈ 150 kHz, respectively. The phosphors used for the DT run (P46) had a natural decay time of $< 1\ \mu\text{s}$, and so were not a limiting factor in the time response of the system. The 2-D scintillator light emission patterns which were used to infer the pitch angle versus gyroradius distribution were typically taken with ≈ 1 – 10 ms exposures at a framing rate of ≈ 60 Hz, thus they were not always able to capture transient MHD events.

The standard TFTR fluctuation diagnostics were used to measure the MHD mode activity described in this article. The two main diagnostics were the poloidal and toroidal arrays of magnetic pick-up (Mirnov) loops on the vessel wall, and the ECE measurements of local electron temperature inside the plasma at two toroidal locations. Information from

neutron emission fluctuation measurements was also used [18]. The frequency response of these diagnostics was up to ≈ 200 kHz.

2.2. Previous experimental results

The experimental results concerning interactions between MHD modes and fast ions in tokamaks (up to 1994) were reviewed in Ref. [4]. The phenomena in that review were divided into ‘resonant loss’, in which the frequency of the dominant MHD mode matched some characteristic frequency of the fast ion motion, and ‘non-resonant loss’, in which it did not. The former was mainly associated with collective fast ion loss, which is not relevant to the data described here.

Previous examples of non-resonant transport of fast ions in tokamaks were mainly associated with sawtooth crashes and $m = 2$ modes. For example, sawtooth crashes were observed using a neutron camera to redistribute beam ions in JET [19], and coherent $m = 2$ modes were observed to cause a reduction in the ^3He burnup in PDX [5]. There were also clear observations of the non-resonant loss of fusion products due to collective MHD instabilities driven by NBI ions, for example, decreases in the burnup of 0.8 MeV ^3He ions in PDX associated with the fishbone instability in PBX [20] and the TAE instability in DIII-D [6].

The effects of MHD activity on DD fusion product loss in TFTR have been described and modelled previously [2]. Strong coherent MHD modes were observed to increase the fusion product loss by up to a factor of 5 above the MHD quiescent first orbit loss level in the 90° scintillator detector. Small bursts of fusion product loss were observed at sawtooth crashes, and large bursts just prior to major disruptions. In general, the experimental results for alphas in DT were qualitatively similar to these earlier DD fusion product results, as expected from the fact that the gyroradii of these fusion products are similar.

A few specific observations of MHD induced DT fusion product loss have been described previously. The presence of kinetic ballooning modes (KBMs) was correlated with a factor of 2 increase in the alpha loss in the 90° scintillator detector, and an orbit model was used to explain this [21, 22]. A large alpha loss was seen during major disruptions [16, 23], an effect of ELMs was observed on alpha loss [24], and sawteeth were found to cause alpha loss in discharges at low toroidal field [12].

The only MHD induced effect seen by the confined alpha diagnostics on TFTR was a sawtooth induced redistribution measured by the pellet charge exchange [25] and α -CHERS [26] diagnostics. Although the internal sawtooth induced redistribution of the confined alphas was large, no increased alpha loss was associated with these sawtooth crashes, which occurred after the main NBI heating pulse in $I = 2.0$ MA high toroidal field discharges.

3. Experimental data on MHD induced alpha loss

This section presents experimental data on MHD induced alpha loss in TFTR DT plasmas as measured by the lost alpha scintillator detectors. In general, there were two classes of MHD instabilities in TFTR: coherent modes (such as tearing modes), which had many oscillation periods and normally reached a nearly steady state amplitude, and transient reconnection events (such as sawteeth and disruptions), which were intrinsically non-periodic.

There was a significant degree of shot to shot variability in the MHD activity which made controlled scans of MHD behaviour difficult, given the small number of DT discharges which could be made for any experiment. Therefore, the data set described in this article contains representative examples, but not any systematic scans which could have clarified the underlying physical dependences.

3.1. Typical time dependence of MHD induced alpha loss

Two examples of the coherent MHD induced alpha loss in NBI heated TFTR DT discharges are shown in Figs 1 and 2. Other examples are given in an extended version of the present paper [27] and in an overview of TFTR alpha measurements [28].

The first example, shown in Fig. 1, was from a normal TFTR DT ‘supershot’ with $I = 1.5$ MA, $B = 4.9$ T, $R = 2.45$ m and 16 MW of NBI from 3–4 s (shot 86289). This discharge had a ≈ 0.1 s burst of ≈ 1 kHz coherent MHD near the time of peak fusion power and stored energy. This MHD was identified by the external magnetic loops as a mixture of $m = 2, n = 1$ and $m = 1, n = 1$ components. The MHD induced alpha loss was observed most clearly in the 20° (‘midplane’) scintillator detector, the aperture of which was 2 cm radially inside the geometrical shadow of the outer limiter for this shot. The

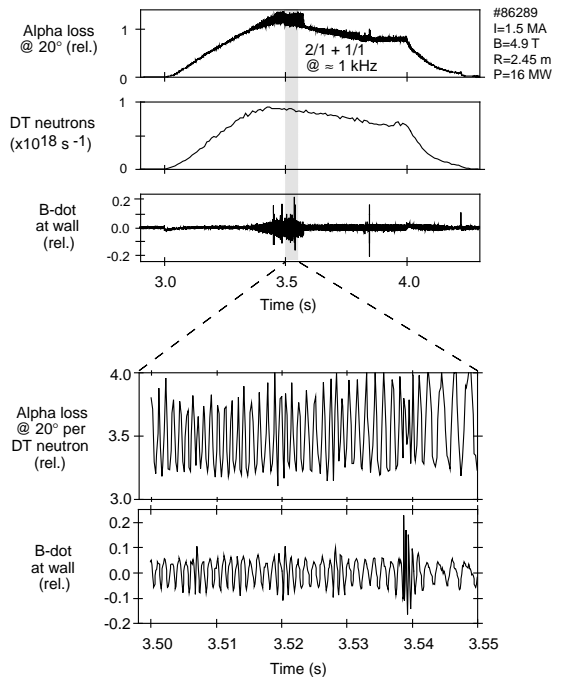


Figure 1. Example of coherent MHD induced alpha loss in a standard TFTR DT supershot with $I = 1.5$ MA and 15 MW of NBI. This discharge had $m = 2, n = 1$ and $m = 1, n = 1$ components at about 1 kHz, which caused an increase in alpha loss by up to $\approx 30\%$ in the midplane detector. The midplane detector aperture in this discharge was at -2 cm with respect to the limiter shadow. The B -dot signal measured the MHD perturbation at the wall.

alpha loss at this detector showed a strong modulation at the frequency of the MHD, with up to a $\approx 30\%$ increase in the peak alpha loss rate and a 15% increase in the alpha loss during this MHD.

The second example, shown in Fig. 2, was a low current discharge from a series of H mode experiments having a current rampdown prior to NBI [24], with $I = 1.0$ MA, $R = 2.45$ m, $B = 4.9$ T and 20 MW of NBI (shot 78607). This case has a series of ‘fishbone’ bursts lasting ≈ 0.2 s near the time of peak fusion power, with each 10 ms long burst consisting of an $m = 1, n = 1$ mode chirping down from ≈ 3 to 0.3 kHz. The largest effect was found in the 90° detector, where the peak alpha loss increased by up to a factor of 2 at a fishbone burst, but the average alpha loss over these bursts increased by only $\approx 15\%$.

In general, coherent MHD induced alpha loss was observed in every one of the detectors in the lost

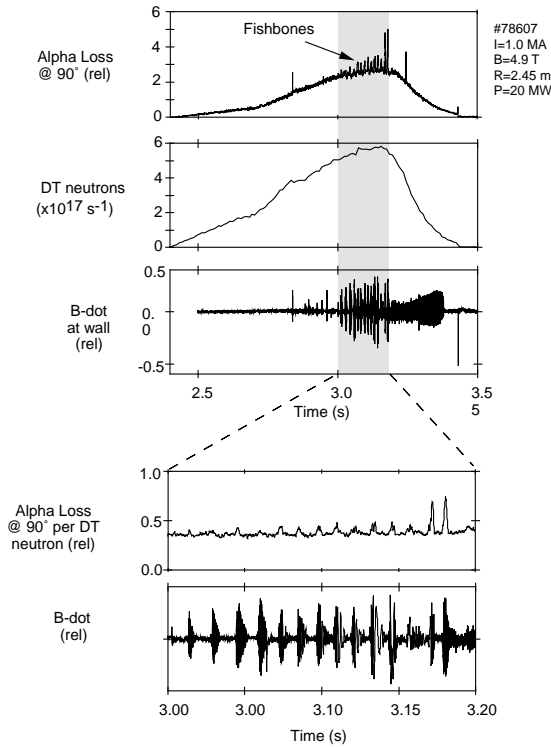


Figure 2. Example of alpha loss caused by fishbone bursts. This discharge was a low current DT super-shot which had a current rampdown prior to NBI in order to induce H modes. Each fishbone burst caused an increase in the alpha loss in the 90° detector of 10–100%, when compared with the MHD quiescent first orbit alpha loss level between bursts. The MHD mode frequency decreased significantly during each burst, and the dominant mode number was $m = 1, n = 1$.

alpha poloidal array, but its poloidal location varied with the details of the MHD activity and/or discharge conditions. The magnitude of the coherent MHD induced alpha loss was generally comparable to or less than the MHD quiescent level of alpha loss.

Two examples of the time dependence of alpha loss during MHD reconnection events are shown in Figs 3 and 4. Other examples are also given in Ref. [27].

Alpha loss during a minor disruption is shown in Fig. 3. This case had $I = 2.5$ MA, $B = 5.1$ T, $R = 2.52$ m and 30 MW of NBI, with a peak fusion power of ≈ 7.5 MW (shot 76773). The alpha loss rate in the 90° detector increased by up to a factor of ≈ 6 within a time of $\leq 100 \mu\text{s}$, as shown at the

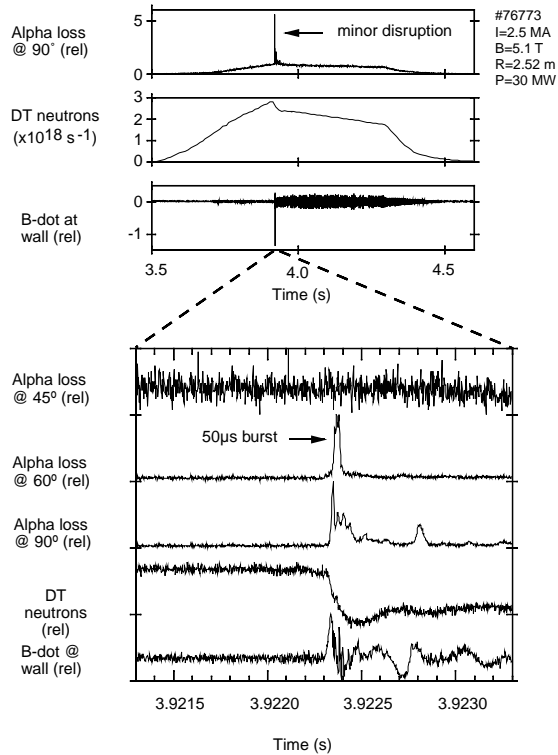


Figure 3. Example of the effect of a minor disruption on alpha loss in a discharge with $I = 2.5$ MA and 30 MW of NBI near the beta limit. The minor disruption caused a drop of $\approx 20\%$ in the neutron rate within ≈ 0.1 ms, during which time the alpha loss increased by a factor of ≈ 6 in the 90° detector. The 60° detector showed a very brief burst of alpha loss, while the 45° detector showed no perceptible loss. The 20° detector was not inserted during this discharge.

bottom of the figure, but the time averaged alpha loss over a period of 5 ms around this time is only $\approx 10\%$ higher than the alpha loss before this event. This type of instability is less severe than a major disruption, since the plasma current remains, but more severe than a sawtooth crash, as it causes a drop of $\approx 20\%$ in the neutron rate. Similar events are observed near the beta limit in many TFTR conditions, including the shot with the TFTR record fusion power (shot 80539).

The effect of a sawtooth crash on alpha loss is illustrated in Fig. 4 for a high toroidal field discharge with $I = 1.4$ MA, $B = 4.9$ T, $R = 2.52$ m and 15 MW of NBI (shot 79175). This shot had a single large sawtooth near the peak of the DT neutron rate, during which there was a large burst of alpha

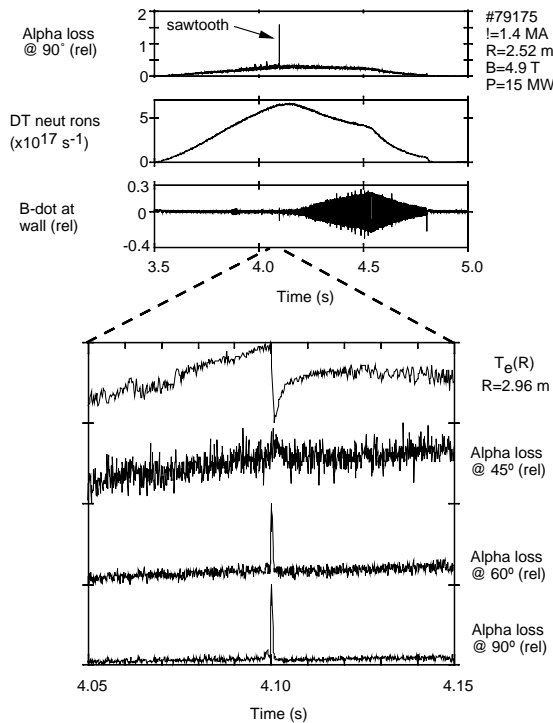


Figure 4. Example of the effect of a sawtooth crash on alpha loss during a moderate powered sawtooth super-shot with $I = 1.4$ MA and 15 MW NBI. In this case the single sawtooth crash caused a factor of 5 increase in the alpha loss at 90° and less of an increase in the 60° and 45° detectors.

loss in the 90° and 60° detectors, but relatively little alpha loss in the 45° detectors. Qualitatively similar behaviour was seen during sawteeth at lower toroidal field and beam heating power [12, 13]. Despite these examples, sawteeth do not normally occur in NBI heated TFTR discharges, and not all DT discharges with sawteeth have bursts of alpha loss [28].

In general, the alpha loss during these transient reconnection events can increase by a factor of up to ≈ 1000 above the MHD quiescent level for a short period of time, ≈ 0.1 – 1 ms. The detailed time structure of the MHD reconnection events and the corresponding alpha loss is complex and not entirely reproducible in detail from shot to shot, perhaps due to a varying toroidal localization of the reconnection processes.

3.2. Pitch angle and gyroradius dependences

Data on the pitch angle and gyroradius distributions of the alpha loss were obtained from the 2-D

pattern of alpha loss onto the scintillator screens, as measured using a gated intensified video camera. Two examples of the pitch and gyroradius distributions of MHD induced alpha loss are shown in Figs 5 and 6. Other examples are in Ref. [27].

Figure 5 shows the effect of a major disruption on the 2-D patterns of alpha loss to the 20° and 90° detectors for a discharge with plasma parameters similar to those of Fig. 2. The instantaneous alpha loss in the 90° detector increased by a factor of ≈ 1000 in this case, while the alpha loss in the 20° detector increased by a factor of ≈ 10 . The 90° detector shows a large loss of partially thermalized alphas during the disruption, when compared with the pre-disruption pattern, with the peak of the inferred alpha energy spectrum at ≈ 2.5 MeV compared with 3.5 MeV before the disruption. There is a similar but smaller contribution from partially thermalized alphas lost in the 20° detector during disruption. Note that the scintillator light output is linearly proportional to the alpha energy, so these raw data signals are linearly weighted towards the high energy end of the alpha particle energy spectrum.

Figure 6 shows the effect of a sawtooth crash on the pitch and gyroradius distributions for the case of Fig. 4. The pitch angle distribution in the 90° detector shows a peak near the passing–trapped boundary (61°), as expected from the conversion of passing alphas to trapped alphas [11–13]. The alpha gyroradius distribution does not change significantly during the crash, indicating that the sawtooth induced alpha loss consists of nearly birth energy alphas.

3.3. Variations in the MHD induced alpha loss at 90°

A database of 21 examples similar to those described in Section 3.1 was used to evaluate the variations in MHD induced alpha loss [27]. This section describes the variations observed at the 90° poloidal detector. The poloidal dependence and the absolute alpha loss fraction are discussed in succeeding sections.

Figure 7 shows the maximum level of the time dependent MHD induced alpha loss rate as measured in the 90° scintillator detector for these discharges. The horizontal axis is a characterization of the type of MHD, and the vertical axis is the peak alpha loss rate normalized by the DT neutron rate at that time. The MHD quiescent alpha signal level corresponding to the first orbit loss [16] is subtracted out in all cases, but its relative level is shown separately by

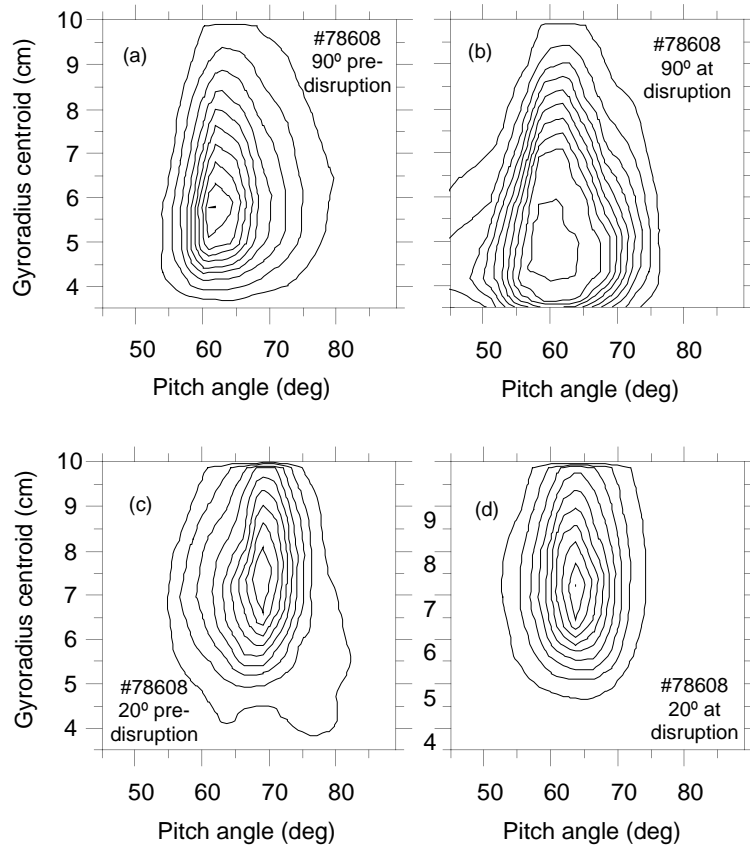


Figure 5. Pitch angle versus gyroradius distributions in the 90 and 20° detectors during a major disruption. There is a significant component of partially thermalized alpha loss observed during the disruption in the 90° detector and a less significant one in the 20° detector. This discharge had parameters similar to those indicated in Fig. 2.

the shaded region near the bottom of the figure. This first orbit loss rate decreases by about a factor of 5 over the plasma current range of $I = 1.0$ MA to $I = 2.7$ MA in this data set.

Figure 7 shows that major disruptions caused the largest peak alpha loss rate in the 90° detector, and that coherent MHD caused the smallest increase in the alpha loss rate. Specifically, the alpha loss rate increased by a factor of ≈ 100 – 1000 above the first orbit loss level during major disruptions, but only by an amount comparable to the first orbit loss level during coherent MHD. Minor disruptions and sawtooth crashes caused an intermediate increase by a factor of ≈ 10 above the first orbit loss level.

Such variations in the MHD induced alpha loss are presumably due to the variability of the internal

magnetic perturbations. These perturbations were measured using the ECE diagnostic, which provided a radial profile of the electron temperature versus time used to estimate the internal displacement of the magnetic field lines, i.e. the magnetic island width. The externally measured magnetic fluctuations were also used to determine the poloidal and toroidal mode numbers m and n . Most of the coherent MHD modes in Fig. 7 had low mode numbers $m = 1$ – 3 and island widths of 2–10 cm, except for the high frequency KBMs that typically had $m \approx 6$ and a displacement of ≈ 1 cm.

In this database there was only a moderate correlation between the size of the estimated magnetic island width and the level of MHD induced alpha loss [27], and no single plasma or MHD parameter was

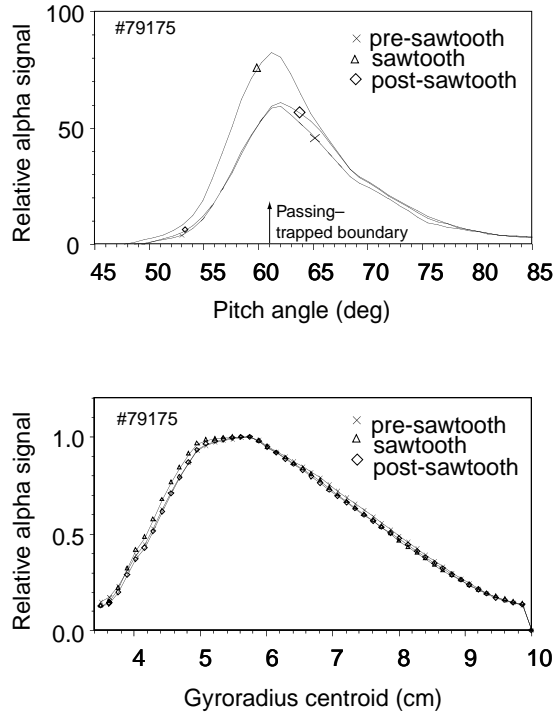


Figure 6. Pitch angle and gyroradius distributions observed in the 90° detector during a sawtooth crash in the discharge of Fig. 4. The sawtooth induced alpha loss occurred near the passing-trapped boundary at 61° pitch angle, but with a gyroradius distribution not significantly different from that observed before or after the sawtooth crash.

found which correlated well with the MHD induced alpha loss over the whole data set [27]. This is most likely due to a sensitivity of the alpha loss to the details of the internal structure of the magnetic field perturbations, which are not well measured.

3.4. Poloidal distribution of the MHD induced alpha loss

The poloidal distributions of the MHD induced alpha loss in this database is shown in Fig. 8. The vertical axis represents the magnitude of the peak MHD induced alpha loss in each detector, after subtracting out the MHD quiescent alpha loss level and normalizing by the DT neutron rate (as in Fig. 7). The relative detector efficiencies are taken into account so that the various poloidal angles and shots can be directly compared with each other. Only the alpha loss levels from the three fixed detectors at

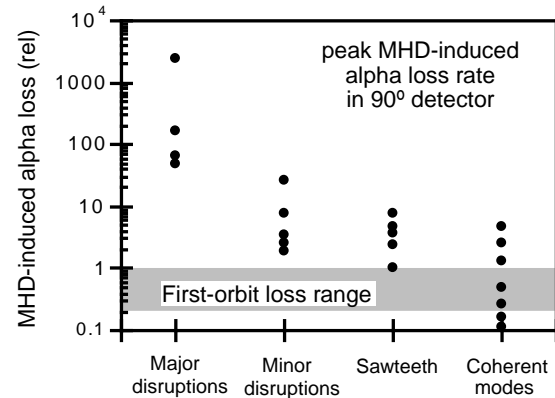


Figure 7. Peak MHD induced alpha loss rate as measured in the 90° detector for various types of MHD activity. Each point represents one shot, and all the data are normalized to the DT neutron rate at the time of the MHD. The MHD quiescent first orbit alpha loss has been subtracted from the data, but is shown separately by the shaded region (its range is due to the varying plasma currents). For example, during major disruptions the instantaneous alpha loss during disruptions can be up to 1000 times the first orbit loss.

45, 60 and 90° below the outer midplane are plotted, since the signal level for the movable 20° detector depended on the radial position of the detector.

The poloidal distributions for most of the reconnection events such as major and minor disruptions and sawtooth crashes were peaked at the 90° detector, with the remainder slightly peaked at the 60° detector, and with all cases having at least an order of magnitude lower signal at the 45° detector. For the coherent MHD modes there is a wider range of behaviour, with some cases strongly peaked at the 45° detector or the 60° detector, but most fairly uniform in poloidal angle.

The 20° (outer midplane) alpha detector data were not used in Fig. 8 since its radial position varied from shot to shot. As discussed in Ref. [27], the ratio of the MHD induced alpha loss in the 20° detector to that in the 90° detector increased as the 20° detector aperture was moved inwards, similar to the trend seen in MHD quiescent alpha loss [17]. However, even at a fixed radial position there was at least a factor of 10 variation of the $20^\circ/90^\circ$ MHD induced alpha loss ratio, depending on the type of discharge and type of MHD activity.

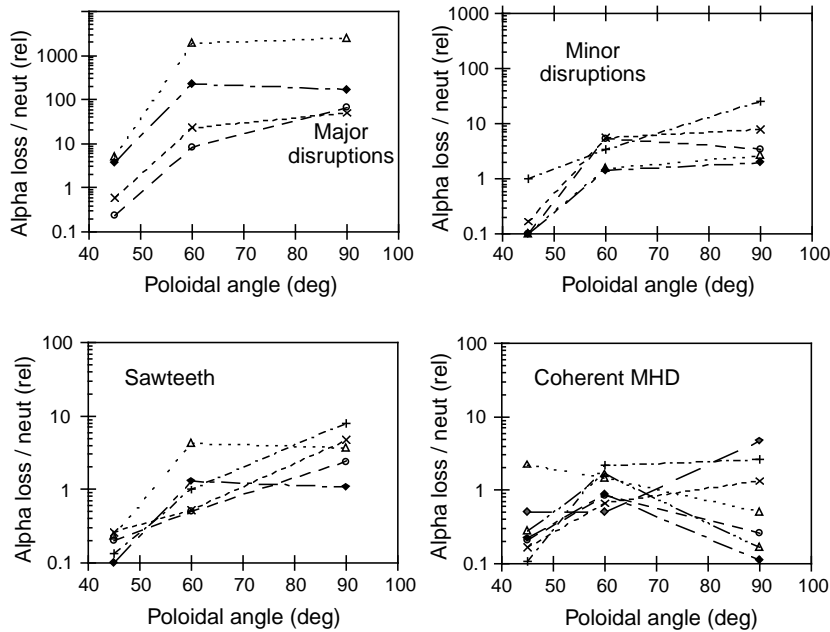


Figure 8. Poloidal distributions of MHD induced alpha loss for the same data set shown in Fig. 7. The poloidal distributions are generally peaked towards the bottom of the vessel for reconnection events (disruptions and sawteeth) but are broader and more variable for the coherent MHD modes. The vertical scales are the same as those for Fig. 7. The first orbit loss level is between 0.1 and 1 for this range of poloidal angles (depending on the plasma current).

3.5. Estimate of the total alpha loss fraction

An estimate of the total alpha loss fraction due to these MHD induced alpha loss events is shown in Fig. 9, based on the MHD data set of Figs 7 and 8. The vertical axis F_{MHD} is the estimated fraction of the confined alphas which are lost to the wall due to these MHD events, as obtained from the available data using the following formulas:

$$F_{MHD} \approx M f_{fo} (\tau_{MHD} / \tau_{s_\alpha}) / 2 \text{ for } \tau_{MHD} < \tau_{s_\alpha} \quad (1a)$$

$$F_{MHD} \approx M f_{fo} / 2 \text{ for } \tau_{MHD} > \tau_{s_\alpha} \quad (1b)$$

where M is a multiplication factor expressing the poloidal average of the MHD induced loss rate in the units of Fig. 8, where the first orbit loss rate was taken to be ‘1’ (as in Fig. 7). Here f_{fo} is the global first orbit alpha loss fraction taken from Monte Carlo calculations [16], τ_{MHD} is the duration of the MHD events [27] and τ_{s_α} is the average alpha thermalization time inside the plasma, which is taken to be 0.1 s for all cases [17]. The factor of 2 in the denominator takes into account the fact that the M 's are the

peak values in time and not time averages (this tends to overestimate F_{MHD} for coherent modes). In the limit where $\tau_{MHD} / \tau_{s_\alpha} > 1$ (e.g. for steady coherent modes), the MHD induced loss can be calculated as a simple multiplier of the first orbit loss, based on the measured ratio M for the MHD induced to MHD quiescent alpha loss. In the limit where $\tau_{MHD} / \tau_{s_\alpha} < 1$ (e.g. for reconnection events), the duration of the MHD induced loss is normalized to the total alpha population in the discharge integrated over its thermalization time of τ_{s_α} .

The implication of Fig. 9 is that the largest MHD induced alpha loss fraction occurred during major disruptions when typically $F_{MHD} \approx 1\text{--}10\%$ of the alphas in the discharge were lost to the wall in $\approx 0.1\text{--}1$ ms just prior to the current quench. The alpha loss fractions F_{MHD} due to minor disruptions or sawtooth crashes were estimated to be in the range $\approx 0.01\text{--}0.1\%$, and those for coherent modes to be in the range $\approx 0.1\text{--}10\%$, such that the highest levels for coherent MHD induced alpha loss were comparable to the highest first orbit loss levels. There is a

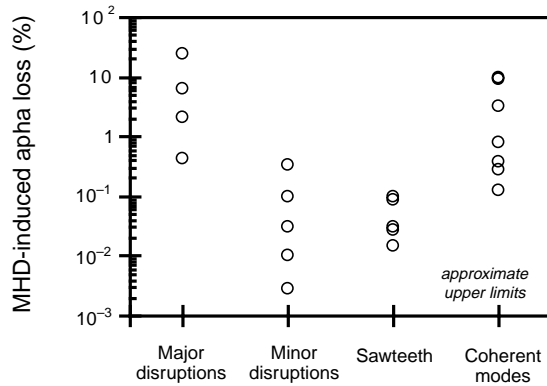


Figure 9. Estimate of the MHD induced alpha loss fraction for various types of MHD activity in TFTR, averaged over the three fixed poloidal detectors and the duration of the MHD activity. The vertical scales are order of magnitude estimates for the alpha loss fractions; for example, the alpha loss during a single sawtooth event is $<0.01\%$, i.e. negligible with respect to that during a major disruption.

discussion of a wider database of MHD induced alpha loss in Ref. [27]; the cases in Fig. 9 represent the strongest MHD induced alpha losses of each type seen in TFTR.

Of course, these F_{MHD} are only order of magnitude estimates given the approximations used in Eq. (1), particularly since only a small fraction of the wall area was used to estimate the factor M . However, one confirming measurement is that described in Ref. [26] where alpha loss due to a sawtooth crash as estimated from α -CHERS was found to be negligible, which is consistent with Fig. 9.

4. Modelling

The modelling of MHD induced alpha loss is the same as applied previously for DD and $D^3\text{He}$ fusion products [2, 5] and NBI ions [29], since this is a ‘single particle’ interaction, i.e. independent of the number of fast ions. The challenge in understanding the present results lies in the incompleteness of the data on both the internal MHD structure and on the alpha loss.

4.1. Model for coherent MHD induced alpha loss

The most important parameter in the theory of interactions between MHD modes and alpha

particles is the ratio of the alpha gyroradius to the plasma minor radius ρ_α/a , which is also a measure of the alpha banana width for a given plasma shape and $q(r)$ profile. In the limit where $\rho_\alpha/a = 0$, alpha orbits follow field lines and there is no alpha loss. In the limit when $\rho_\alpha/a \geq 0.1$, a significant MHD induced alpha loss to the wall may occur due to the MHD induced distortion of closed alpha drift orbits [5]. In between these limits, which is the normal range for coherent modes in TFTR, stochastic alpha diffusion can occur for both passing and trapped particle orbits [11].

The effect of coherent modes on alpha particle orbits is most easily calculated using a guiding centre code with an internal helical magnetic perturbation. In the analysis below, the ORBIT code [30] is used with simplified magnetic perturbations of the form

$$\delta B = \nabla \times \alpha B_0 \quad (2)$$

where B_0 is the equilibrium field, $\alpha = \sum \alpha_{mn}(r) \times \sin(m\theta - n\phi)$ and $\alpha_{mn}(r) \sim r^m(a - r)$. This produces a relatively broad perturbation which forms an island structure near the chosen rational mode number, but does not produce stochastic magnetic fields. The effect on the alpha orbits comes entirely through the change in the magnetic structure, and is not due to a change in the perturbed curvature drifts (which was also treated in the theory given in Ref. [11]). A single perturbation produces a series of islands in the particle drift surface due to the coupling between the mode and the $n = 0$ orbit shift, which produces stochasticity when these islands overlap.

A Monte Carlo code was used to simulate the effects of coherent modes on the confinement of alpha particles born with random pitch angles and a realistically peaked radial source profile [27]. Typical results for a single large $m = 2$, $n = 1$ island (20 cm island width) at $I = 1.4$ MA are shown in Fig. 10. For this run 3000 alphas were followed for 1000 toroidal transits (it was typically found that for a realistic collisionality over 80% of the eventual alpha loss occurred within 1000 transits). The poloidal loss distribution was peaked between 0 and 60° below the outer midplane, with relatively little alpha loss predicted near 90°. The toroidal distribution shows a significant modulation with toroidal angle for this stationary mode.

The absolute magnitude of calculated alpha loss fractions versus the MHD island width and mode number for $I = 1.4$ MA are shown in Fig. 11. The overall result is that the MHD induced alpha loss fractions increase approximately as the square root

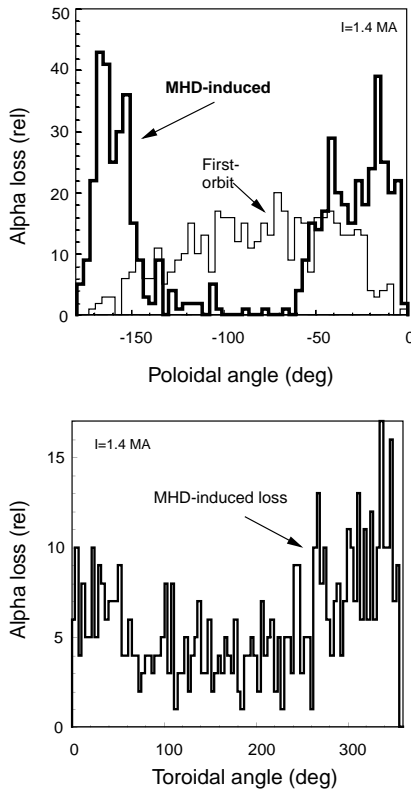


Figure 10. Poloidal and toroidal alpha loss distributions from a Monte Carlo simulation of a coherent $m = 2$, $n = 1$ MHD mode. This case was for $I = 1.4$ MA and a magnetic island width of 20 cm. The poloidal distributions are peaked within $\approx 60^\circ$ below the outer and inner midplanes, corresponding to the loss of co- and counter-going alphas, respectively, with relatively little alpha loss predicted near the bottom of the vessel. The toroidal distribution shows an $\approx 50\%$ modulation of the loss with toroidal angle for this zero frequency mode.

of the island width (or linearly with the internal magnetic field amplitude) for a given mode number. There is a discussion of the comparison with the experimental results in Section 5.1.

4.2. Model for magnetic reconnection induced alpha loss

The theory and modelling of Section 4.2 is not useful for evaluating the effects of magnetic reconnection on alpha loss, since the magnetic structure is probably stochastic and induced electric fields may affect the orbit dynamics [13]. For the sake of a qualitative

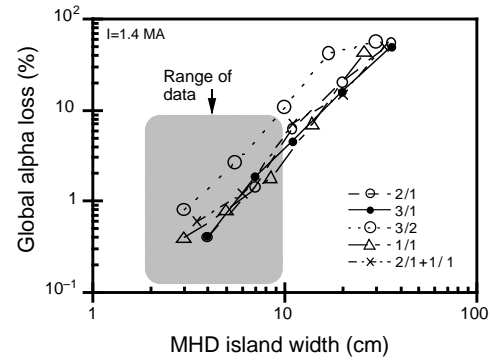


Figure 11. Modelling of the global alpha loss versus mode number and magnetic island width for $I = 1.4$ MA cases. Each point represents a guiding centre code run with 500–5000 alpha particles for 1000 toroidal transits. The range of the experimental data set for coherent modes is shown by the shaded region. This data set contains plasma currents in the range $I = 1.0$ – 2.3 MA, and so does not correspond exactly to these calculations for $I = 1.4$ MA.

understanding of the data, a simplified model for reconnection induced alpha loss is described below.

This model is based on the observation that reconnection induced alpha loss often occurs near the passing–trapped boundary (e.g. Fig. 6) and at the bottom of the vessel (Fig. 8). The maximum possible loss of this type occurs when all confined counter-passing alphas radially inside the passing–trapped boundary move outward and become converted into trapped orbits, whereby they are lost in one poloidal transit to the bottom of the vessel [31]. This process will naturally occur during reconnection, when the magnetic structure near the plasma centre is highly disturbed and the alphas are radially redistributed [26].

This maximum ratio of such a reconnection induced alpha loss rate R_{recon} to the first orbit loss rate R_{fo} is therefore roughly

$$R_{recon}/R_{fo} \approx (\langle S_\alpha \rangle_{in} / \langle S_\alpha \rangle_{out}) (\tau_{s_\alpha} / \tau_{recon}) \quad (3)$$

where τ_{recon} is the time over which this reconnection induced radial transport occurs, τ_{s_α} is the time over which confined alphas slow down in the core region, and $\langle S_\alpha \rangle_{in}$ and $\langle S_\alpha \rangle_{out}$ are the volume averaged alpha source rates in the interior confined region, respectively. There is a discussion of the comparison with the experimental results in Section 5.1.

5. Discussion

The experimental data of Section 3 are compared with the modelling of Section 4 in Section 5.1, the implications for an alpha heated tokamak reactor are discussed in Section 5.2, and the summary is in Section 5.3. More details concerning specific comparisons of experiment and theory are in Ref. [27].

5.1. Comparison of experiment and modelling

The experimental estimates for coherent MHD induced alpha loss fraction (Fig. 9) are compared with the calculated alpha loss fractions for various types of coherent MHD modes in Fig. 11. The experimental estimates of $F_{MHD} \approx 0.1\text{--}10\%$ for global MHD induced alpha loss are at least qualitatively consistent with these simulations, given the measured magnetic island widths of $\approx 2\text{--}10$ cm in experiment.

However, this comparison has considerable uncertainty due to the following factors: uncertainty in the experimental estimates of alpha loss (Section 3.5), oversimplification of the MHD mode structure in the modelling (Section 4.1) and the range of plasma currents in the experiments ($I = 1.0\text{--}2.3$ MA) compared with the single plasma current used in this modelling ($I = 1.4$ MA). Thus, the agreement shown in Fig. 11 should be considered only qualitative. A similar level of agreement was found in an attempt to analyse a specific discharge at $I = 2.3$ MA [28].

For reconnection induced alpha loss only the highly simplified model of Section 4.2 is readily available to compare with the data. Referring to the estimate for the ratio of reconnection induced loss to first orbit loss (Eq. (3)), for either sawtooth or disruptive events, $\tau_{s\alpha}/\tau_{recon} \approx 0.1$ s/0.1 ms ≈ 1000 and $\langle S_\alpha \rangle_{in}/\langle S_\alpha \rangle_{out} \approx 1$ [31]; therefore the maximum possible reconnection induced alpha loss rate should be ≈ 1000 times the first orbit loss rate to the bottom detector. This is similar to the estimated upper limit observed during major disruptions (Fig. 7), but is much higher than that observed during sawteeth. This may be due to the fact that a sawtooth crash only seems to expel alphas near the birth energy (Fig. 6), whereas a major disruption also expels partially thermalized alphas (Fig. 5). Note, however, that this simple model ignores changes in the alpha energy and magnetic moment which can occur when the reconnection timescale is comparable to the alpha transit timescale, as is the case for fast reconnection events [12–14].

The following additional points of comparison between experiment and modelling for coherent modes can also be noted:

- (a) The experimental data often showed a large temporal modulation of the alpha loss rate in phase with a coherent mode (e.g. Fig. 1). The simulation of the toroidal angle dependence of the alpha loss for a stationary mode also showed a large modulation (Fig. 10). Thus the simulation can at least qualitatively explain this observation, assuming the alpha loss at a fixed detector is modulated by the slow (compared with the alpha transit time) toroidally rotating mode.
- (b) The poloidal distribution observed for the reconnection events (Fig. 8) was generally peaked near the bottom of the vessel, roughly consistent with the passing–trapped boundary loss model, and also with detailed MHD simulations [32]. However, the observations of significant coherent MHD induced alpha loss at the bottom of the vessel (Fig. 8) appear not to be consistent with the coherent mode model of Section 4.1, which predicts an alpha loss to be strongly peaked towards the outer midplane (Fig. 10).
- (c) The observation of alpha loss at the passing–trapped boundary during sawtooth reconnection events (e.g. Figs 5 and 6) is at least qualitatively explained by the reconnection based passing–trapped boundary model of Section 4.2.
- (d) The absence of MHD induced alpha loss for the sawteeth which occurred after the turn-off of NBI [25, 28] could be due to the sensitivity of the reconnection induced alpha loss to the location of the passing–trapped boundary with respect to the reconnection region. For example, if the $q = 1$ surface at which the sawtooth induced reconnection occurs is not near the radius of the passing–trapped boundary, the loss will be insensitive to the reconnection induced radial transport [13].
- (e) The similarity between the MHD induced alpha loss for DT alphas and DD fusion products [2] is explained by the single particle models of Section 4, since these ions have similar values of ρ_α/a . This would not be the case if these losses were dominated by collective effects, since the confined alpha population is ≈ 100 times larger than that for DD fusion products.

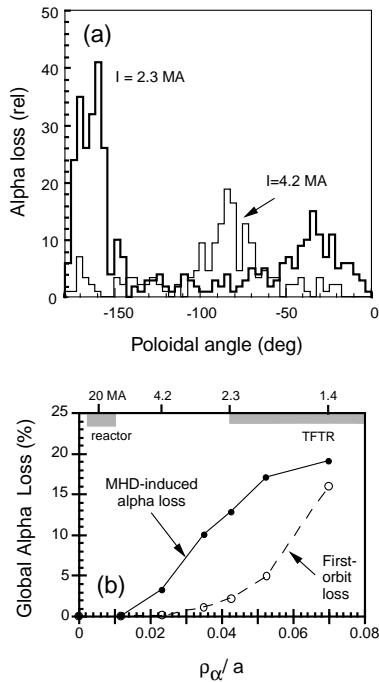


Figure 12. Variation of the calculated MHD induced alpha loss fraction versus ρ_α/a for a fixed ratio of island width to minor radius for a large $m = 2$, $n = 1$ mode (similar to Fig. 10, but with a ρ_α/a varied by changing the birth energy). (a) Poloidal distributions of MHD induced alpha loss for two plasma currents, (b) calculated global MHD induced alpha loss versus ρ_α/a for a TFTR-like plasma geometry. The coherent MHD induced alpha loss should be negligible for reactor relevant ρ_α/a .

5.2. Reactor relevance

It was noted in Section 4.1 that coherent MHD induced alpha loss decreased with ρ_α/a at a fixed $q(a)$ as the alpha drift surfaces became closer to the magnetic flux surfaces. Figure 12 shows a Monte Carlo calculation of the expected ρ_α/a dependence of global alpha loss due to coherent MHD modes. At the reactor level $\rho_\alpha/a \approx 0.01$ ($I = 20$ MA) even a very large island causes only a very small ($\leq 1\%$) global alpha loss and so would have a negligible effect on alpha heating. However, this calculation also shows that the poloidal dependence of the alpha loss tends to become more localized as ρ_α/a decreases (at least for TFTR geometry), implying that the local MHD induced alpha heat loss to the reactor wall should still be examined carefully [33].

The effects of reconnection on alpha loss will not scale simply with ρ_α/a , but will depend upon the details of the MHD. However, even if a large fraction of the alphas were lost during a sawtooth, the plasma would most likely reheat before the thermal energy was lost, unless the period of the sawteeth was comparable to the energy confinement time [34]. Thus, such MHD perturbations do not seem to be particularly dangerous with regard to the loss of ignition in a reactor.

Major disruptions caused the largest MHD induced alpha loss fraction in TFTR, and an analogous loss of $\approx 10\%$ of the confined alphas in a reactor could potentially damage the first wall. However, the confined alphas may well thermalize before they hit the wall of a reactor, since the electron temperature in a thermal quench can be as low as 100 eV. For example, the alpha thermalization time at $n_e = 10^{14} \text{ cm}^{-3}$ and $T_e = 100 \text{ eV}$ is only $\approx 100 \mu\text{s}$, which may be less than the alpha loss time due to the disruption.

5.3. Summary

This article described measurements and modelling of alpha loss due to plasma driven MHD modes in TFTR DT plasmas. For coherent modes the MHD induced alpha loss was similar in magnitude to the MHD quiescent alpha loss. However, for magnetic reconnection events such as sawteeth and disruptions the alpha loss increased by up to ≈ 1000 times the MHD quiescent loss level, but only transiently. For both cases the estimated alpha loss was still a relatively small fraction of the confined alpha population ($\approx 0.1\text{--}10\%$).

There was a qualitative agreement between the experimental results and modelling based on the internal magnetic perturbations. The limitations of this comparison were due to the lack of detailed information on the magnetic structure and also the incomplete spatial resolution in the alpha loss measurements.

On the basis of the results of this article, we infer that the effects of plasma driven MHD modes are not likely to cause a significant loss of alpha heating in a high current tokamak reactor. The most likely cause of alpha heat loss in such reactors would be collective MHD modes driven by the alpha population itself [34]. This type of alpha loss was not observed in TFTR.

Acknowledgements

We thank C.E. Bush, D.W. Johnson, R. Fisher, N. Gorelenkov, W. Heidbrink, Y. Kolesnichenko, S.S. Medley, H.E. Mynick, W. Park, M. Petrov, S. Putvinski, I. Semenov, J.D. Strachan, B.C. Stratton, H. Takahashi and Y. Yakovenko for discussions on this subject, and M. Bell, H.P. Furth, D. Meade, R. Hawryluk and K.M. Young for their support of this work, which was performed under USDOE Contract No. DE-AC02-76-CH03073.

References

- [1] Fredrickson, E.D., et al., in Plasma Physics and Controlled Nuclear Fusion Research 1994 (Proc. 15th Int. Conf. Seville, 1994), Vol. 1, IAEA, Vienna (1995) 275.
- [2] Zweben, S.J., et al., Phys. Plasmas **1** (1993) 1469.
- [3] Nazikian, R., et al., Phys. Rev. Lett. **78** (1997) 2976.
- [4] Heidbrink, W.W., Sadler, G., Nucl. Fusion **34** (1994) 535.
- [5] Heidbrink, W.W., et al., Nucl. Fusion **23** (1983) 917.
- [6] Duong, H., Heidbrink, W.W., Nucl. Fusion **33** (1993) 211.
- [7] Bittoni, E., Haegi, M., Fusion Technol. **22** (1992) 461.
- [8] Sigmar, D.J., et al., Phys. Fluids B **4** (1992) 1506.
- [9] White, R.B., Mynick, H.E., Phys. Fluids B **1** (1989) 980.
- [10] Konovalov, S., Putvinski, S.V., Fusion Technol. **18** (1990) 397.
- [11] Mynick, H.E., Phys. Fluids B **5** (1993) 3490.
- [12] Kolesnichenko, Ya., et al., Phys. Plasmas **6** (1999) 1117.
- [13] Kolesnichenko, Ya., et al., IAEA-CN-69/THP/2, paper presented at 17th IAEA Conf. on Fusion Energy, Yokohama, 1997.
- [14] Gorelenkov, N.N., et al., Nucl. Fusion **37** (1997) 1053.
- [15] Darrow, D.S., et al., Rev. Sci. Instrum. **66** (1995) 476.
- [16] Zweben, S.J., et al., Nucl. Fusion **35** (1995) 893.
- [17] Zweben, S.J., et al., Nucl. Fusion **38** (1998) 739.
- [18] von Goeler, S., et al., Rev. Sci. Instrum. **57** (1996) 473.
- [19] Marcus, F.B., et al., Plasma Phys. Control. Fusion **33** (1991) 277.
- [20] Heidbrink, W.W., et al., Phys. Rev. Lett. **53** (1984) 1905.
- [21] Chang, Z., et al., Phys. Plasmas **5** (1998) 1076.
- [22] Chang, Z., et al., Phys. Rev. Lett. **76** (1996) 1071.
- [23] Mirnov, S., et al., Phys. Plasmas **5** (1998) 3950.
- [24] Bush, C.E., et al., Phys. Plasmas **2** (1995) 2366.
- [25] Medley, S.S., et al., Nucl. Fusion **38** (1998) 1283.
- [26] Stratton, B.C., et al., Nucl. Fusion **36** (1996) 1586.
- [27] Zweben, S.J., et al., MHD-Induced Alpha Particle Loss in TFTR, Rep. PPPL-3340, Princeton Plasma Physics Lab., NJ (1999) (<http://www.pppl.gov/>).
- [28] Stratton, B.C., et al., Nucl. Fusion. (in press).
- [29] Forest, C.B., et al., Phys. Rev. Lett. **79** (1997) 427.
- [30] White, R.B., Chance, M.S., Phys. Fluids **27** (1984) 2455.
- [31] Zweben, S.J., et al., Nucl. Fusion **31** (1991) 2219.
- [32] Park, W., et al., Phys. Rev. Lett. **75** (1995) 1763.
- [33] Putvinski, S.V., et al., Nucl. Fusion **38** (1998) 1275.
- [34] Romanelli, F., et al., ITER Physics Basis, Nucl. Fusion (in press).

(Manuscript received 26 February 1999

Final manuscript accepted 15 June 1999)

E-mail address of S.J. Zweben: szweben@pppl.gov

Subject classification: F3, Te; D2, Te